



Inflation, space-borne interferometers and the expansion history of the Universe

Massimo Giovannini^{1,2,a}

¹ Department of Physics, CERN, 1211 Geneva 23, Switzerland

² INFN, Section of Milan-Bicocca, 20126 Milan, Italy

Received: 16 June 2022 / Accepted: 10 September 2022 / Published online: 19 September 2022
© The Author(s) 2022

Abstract According to the common wisdom, between a fraction of the mHz and few Hz the spectral energy density of the inflationary gravitons can be safely disregarded even assuming the most optimistic sensitivities of the space-borne detectors. In this analysis we show that this conclusion is evaded if, prior to nucleosynthesis, the post-inflationary evolution includes a sequence of stages expanding either faster or slower than radiation. As a consequence, contrary to the conventional lore, it is shown that below a fraction of the Hz the spectral energy density of the relic gravitons may exceed (even by eight orders of magnitude) the signal obtained under the hypothesis of radiation dominance throughout the whole expansion history prior to the formation of light nuclei. Since the slopes and the amplitudes of the spectra specifically reflect both the inflationary dynamics and the subsequent decelerated evolution, it is possible to disentangle the contribution of the relic gravitons from other (late-time) bursts of gravitational radiation associated, for instance, with a putative strongly first-order phase transition at the TeV scale. Hence, any limit on the spectral energy density of the relic gravitons in the mHz range simultaneously constrains the post-inflationary expansion history and the inflationary initial data.

1 Introduction

A striking prediction of the early evolution of the space-time curvature is the formation of a stochastic background of relic gravitons [1–4] whose frequencies may extend between the aHz and the GHz regions. As originally pointed out in Refs. [5,6], the spectral energy density of relic gravitons is quasi-flat between 100 aHz and 100 MHz for the inflationary scenarios relying on the conventional slow-roll evolution. Since

the quasi-flat plateau corresponds to wavelengths that left the Hubble radius during inflation and reentered after radiation was already dominant, the spectral energy density can only reach its maximum in the aHz region where the signal scales as ν^{-2} with the comoving frequency ν [7]. In the aHz interval the temperature and the polarization anisotropies of the cosmic microwave background are customarily employed to infer the tensor to scalar ratio r_T here assumed in the range $r_T = r_T(\nu_p) \leq 0.06$, as suggested by recent determinations [13–15]. For the record $\nu_p = k_p/(2\pi) = 3.09$ aHz and $k_p = 0.002$ Mpc⁻¹ denotes the pivot scale at which the scalar and tensor power spectra are conventionally assigned when the relevant wavelengths are larger than the Hubble radius prior to matter-radiation equality.

Depending on the value of r_T , the spectral energy density in critical units¹ well above 100 aHz is $h_0^2 \Omega_{gw}(\nu, \tau_0) < \mathcal{O}(10^{-17})$ and this estimate includes the effect of the various damping source such as the late-dominance of the dark energy, the evolution of the relativistic species and the free-streaming of the neutrinos [16,17]. For all these reasons the spectral energy density of inflationary origin is too small to be detected by either ground based or space-borne detectors even in their most advanced versions. At the moment the only direct bounds on the relic gravitons come from the audio band and depend upon the spectrum of the signal but we

¹ Instead of working with the spectral energy density of the relic gravitons in critical units (conventionally denoted by $\Omega_{gw}(\nu, \tau_0)$) it is practical to introduce $h_0^2 \Omega_{gw}(\nu, \tau_0)$ where h_0 is the indetermination of the Hubble rate. The spectral energy density of the relic gravitons *does not* coincide with their energy density in critical units which is instead frequency-independent. We also note that the frequencies are often mentioned in the text by using the standard metric prefixes of the international system of units. So, for instance, aHz = 10⁻¹⁸ Hz, mHz = 10⁻³ Hz and so on. After the analysis of Refs. [5,6] suggesting a flat slope for $\Omega_{gw}(\nu, \tau_0)$ various authors discussed the same problem with a number of relevant additions; in this respect the interested reader may consult Refs. [8–12].

^a e-mail: massimo.giovannini@cern.ch (corresponding author)

could anyway say that, for a nearly scale-invariant spectrum, $h_0^2 \Omega_{gw}(\nu, \tau_0) < \mathcal{O}(10^{-9})$ between 10 Hz and 80 Hz [18, 19] (see also [20] for a recent review including earlier bounds). For a physical comparison between the ground-based detectors and the (futuristic) space-borne interferometers the spectral energy density can be usefully expressed in terms of the chirp amplitude $h_c(\nu, \tau_0)$ [20] when the typical frequencies fall in the audio band:

$$h_0^2 \Omega_{gw}(\nu, \tau_0) = 6.26 \times 10^{-9} \left(\frac{\nu}{0.1 \text{ kHz}} \right)^2 \left[\frac{h_c(\nu, \tau_0)}{10^{-24}} \right]^2. \quad (1.1)$$

If we read Eq. (1.1) from left to right we can argue that to probe $h_0^2 \Omega_{gw}(\nu, \tau_0) = \mathcal{O}(10^{-9})$ we would need a sensitivity in the chirp amplitude $\mathcal{O}(10^{-24})$ for a typical frequency $\nu = \mathcal{O}(100)$ Hz. From right to left Eq. (1.1) suggests instead that, for the same sensitivity in $h_c(\nu, \tau_0)$, the minimal detectable $h_0^2 \Omega_{gw}(\nu, \tau_0)$ gets comparatively smaller². This is why the minimal detectable spectral energy density could be $h_0^2 \Omega_{gw}(\nu, \tau_0) = \mathcal{O}(10^{-11})$ or even $h_0^2 \Omega_{gw}(\nu, \tau_0) = \mathcal{O}(10^{-15})$ under the hypothesis that the same sensitivity reached in the audio band for the chirp amplitude can also be achieved in the mHz range. With this hope, various space-borne detectors have been proposed so far: the Laser Interferometric Space Antenna (LISA) [21, 22], the Deci-Hertz Interferometer Gravitational Wave Observatory (DECIGO) [23, 24], the Ultimate-DECIGO [25] (conventionally referred to as U-DECIGO), the Big Bang Observer (BBO) [26]. This list has been recently enriched by the Taiji [27, 28] and by the TianQin [29, 30] experiments. Since these instruments are not yet operational (but might come into operation within the next twenty years) their actual sensitivities are difficult to assess, at the moment. However, without dwelling on the specific nature of the noise power spectra, Eq. (1.1) shows that, as long as $h_c = \mathcal{O}(10^{-23})$ the space-borne detectors might probe $h_0^2 \Omega_{gw}(\nu, \tau_0) = \mathcal{O}(10^{-14})$ for $\nu_S = \mathcal{O}(0.01)$ Hz and this is, roughly speaking, the daring expectation of DECIGO [23, 24] and of U-DECIGO [25].

According to the standard lore (see e.g. [21–24]) the astrophysical sources of gravitational radiation (i.e. mostly white dwarves and solar masses black holes) dominate the signal below 0.1 Hz, while the bursts of gravitons from the TeV physics are unlikely in the standard electroweak theory but should be anyway subleading in comparison with the galactic foregrounds. Because of the relative smallness of its spectral energy density, the inflationary background of relic gravitons is always disregarded but this conclusion is only based on a specific expansion history and it can be evaded if, prior to nucleosynthesis, the evolution of the background is not

constantly dominated by radiation. Indeed, the flatness of $h_0^2 \Omega_{gw}(\nu, \tau_0)$ for frequencies larger than 100 aHz is not only determined by the inflationary evolution when the relevant wavelengths exit the Hubble radius but also by the expansion rate at reentry [31, 32]. The high-frequency signal is maximized by a long stage expanding at a rate that is slower than radiation [31, 32] and this possibility is realized in various classes of quintessential inflationary scenarios [33, 35–37] (see also [38, 39]). The signal from a long stiff phase does not imply a reduction of $h_0^2 \Omega_{gw}(\nu, \tau_0)$ in the aHz region so that the high-frequency measurements of wide-band detectors and the low-frequency determinations of r_T can be simultaneously constrained within an accurate numerical framework [40, 41]. In this context the potential signal might be sufficiently large both in the aHz region and in the audio band.

While in the case of a stiff post-inflationary phase the spike typically arises for frequencies between the GHz and 100 GHz it is also possible to have different profiles of the spectral energy density with a number of different peaks when the frequency is comparatively smaller or even much smaller than the MHz. There is then a trade-off between the smallness of the frequency and the magnitude of $h_0^2 \Omega_{gw}(\nu, \tau_0)$ [40, 41]. Since the most general post-inflationary expansion rate consists of a series of successive stages expanding at different rates that are either faster or smaller than radiation³ [40–42], in this paper we are going to argue that the general approach previously explored is also applicable also to smaller frequencies in the mHz region. In the presence of a modified post-inflationary expansion rate the standard inflationary signal computed in Refs. [5–7] can be much larger below the Hz and potentially dominant against the bursts of gravitational radiation from strongly first-order phase transitions.

The layout of this paper is the following. In Sect. 2 the inflationary power spectra are computed after the relevant wavelengths reentered the Hubble radius during a post-inflationary stage that differs from radiation. In Sect. 3 we examine the general case where each stage of a larger sequence of phases expands at a rate that is either faster or slower than radiation. In this situation the spectral energy density exhibits a succession of peaks and troughs whose frequencies are solely determined by the curvature scale. Since the slopes of the humps in $h_0^2 \Omega_{gw}(\nu, \tau_0)$ depend both on the inflationary stage and on the post-inflationary evolution, in Sect. 4 it is shown that the current limits from ground-based detectors already pin down a well defined region of the

² Besides the the absence of seismic noise this is probably one of strongest arguments in favour of space-borne detectors for typical frequencies ranging between a fraction of the mHz and the Hz.

³ Incidentally, within the present approach the possibility of a signal in the nHz band (recently suggested by the pulsar timing arrays [43–46]) has been specifically scrutinized by considering a wide range of possibilities including the presence of late-time stages of inflationary expansion [42]. In this paper we are instead concerned with the mHz range and the potential signal from pulsar timing arrays will not be specifically discussed.

parameter space that should be further explored by space-borne interferometers. Section 5 contains the concluding remarks and some comments on the future perspectives.

2 Spectral energy density of the inflationary gravitons

The effect of the post-inflationary evolution is not, as sometimes argued, a purely kinematical problem that is virtually disentangled from the dynamical evolution of the tensor modes. On the contrary the enhancement of the spectral energy density at late times is also determined by the early expansion: it is because of the successive occurrence of an inflationary stage and of the late post-inflationary evolution that $\Omega_{gw}(k, \tau)$ may be enhanced at high and intermediate frequencies [31, 32]. The flat spectrum of relic gravitons for frequencies larger than 100 aHz only arises if the relevant wavelengths exit the Hubble radius during inflation and reenter in a radiation-dominated stage of expansion, as originally assumed in Refs. [5–7]. We may consider, in this respect the standard form of the spectral energy density in critical units that can be written as [20]:

$$\Omega_{gw}(k, \tau_0) = \frac{1}{24H^2 a^2} \left[Q_T(k, \tau) + k^2 P_T(k, \tau) \right], \quad (2.1)$$

where $a(\tau)$ is the scale factor of a conformally flat background geometry, τ is the conformal time and H is the standard Hubble expansion rate. In Eq. (2.1) $Q_T(k, \tau)$ and $P_T(k, \tau)$ are the tensor power spectra that are defined from the evolution of the mode functions $G_k(\tau)$ and $F_k(\tau)$:

$$\begin{aligned} Q_T(k, \tau) &= \frac{4\ell_P^2}{\pi^2} k^3 |G_k(\tau)|^2, \\ P_T(k, \tau) &= \frac{4\ell_P^2}{\pi^2} k^3 |F_k(\tau)|^2, \end{aligned} \quad (2.2)$$

where $\ell_P = \sqrt{8\pi G}$; in what follows the notations for the Planck mass are given by $\bar{M}_P = M_P/\sqrt{8\pi} = 1/\ell_P$ and \bar{M}_P is the reduced Planck mass.

The rescaled mode functions $f_k(\tau) = a(\tau)F_k(\tau)$ and $g_k(\tau) = a(\tau)G_k(\tau)$ obey, in the present context, the standard evolution equations:

$$f_k'' + \left[k^2 - \frac{a''}{a} \right] f_k = 0, \quad g_k = f_k' - \mathcal{H} f_k. \quad (2.3)$$

In Eq. (2.3) the prime denotes a derivation with respect to the conformal time coordinate τ ; we also use the standard notation $\mathcal{H} = aH$ where $\mathcal{H} = a'/a$ and H is the conventional Hubble rate. Within the WKB approximation Eq. (2.3) is approximately solved in the two complementary regimes where k^2 is either larger or smaller than $|a''/a|$. In particular when $k^2 \gg |a''/a|$ the mode functions (f_k, g_k) oscillate while (F_k, G_k) are also suppressed as $1/a$. In the opposite regime (i.e. $k^2 \ll |a''/a|$) $f_k(\tau)$ is said to be superadiabatically amplified, according to the terminology originally

introduced in Refs. [1–3]. The oscillating and the superadiabatic regimes are separated by a region where the solutions change their analytic behaviour and these turning points are defined as solutions of the approximate equation $k^2 \simeq |a''/a|$ that can also be rewritten as:

$$k^2 = a^2 H^2 \left[2 - \epsilon(a) \right], \quad \epsilon(a) = -\frac{\dot{H}}{H^2}. \quad (2.4)$$

During the inflationary stage of expansion $\epsilon \ll 1$ denotes the standard slow-roll parameter; conversely in the post-inflationary phase the background decelerates (but still expands) and $\epsilon(a) = \mathcal{O}(1)$. If $\epsilon \neq 2$ both turning points are regular and this means that Eq. (2.4) can be approximately solved by $k \simeq aH$. For instance when a given wavelength crosses the Hubble radius during inflation we have that $\epsilon \ll 1$ and $k \simeq a_{ex} H_{ex}$ that also means, by definition, $k\tau_{ex} \simeq 1$. Similarly if the given wavelength reenters in a decelerated stage of expansion different from radiation we also have that $k \simeq a_{re} H_{re}$. Finally if the reentry occurs in the radiation stage we have that $\epsilon_{re} \rightarrow 2$ and the condition (2.4) implies that $k\tau_{re} \ll 1$.

These considerations suggest that the spectral energy density of the relic gravitons depends both on the exit and on the reentry of the given wavelength and for this purpose it is appropriate to express the mode functions in the Wentzel–Kramers–Brillouin (WKB) approximation under the further assumption that $a_{re} \gg a_{ex}$: this requirement is verified as long as the Universe expands as it is always the case throughout the present discussion. The initial conditions for the evolution of the mode functions are then assigned during the inflationary stage and before the corresponding wavelengths exit the Hubble radius; in this regime $f_k(\tau)$ and $g_k(\tau)$ are simply plane waves obeying the Wronskian normalization condition:

$$f_k(\tau) g_k^*(\tau) - f_k^*(\tau) g_k(\tau) = i, \quad (2.5)$$

as required by the canonical commutation relations of the corresponding field operators [20]. From the continuity of the mode functions across the turning points of the problem, the expression of $F_k(\tau)$ becomes:

$$\begin{aligned} F_k(\tau) &= \frac{e^{-ik\tau_{ex}}}{a\sqrt{2k}} \mathcal{Q}_k(\tau_{ex}, \tau_{re}) \left(\frac{a_{re}}{a_{ex}} \right) \\ &\times \left\{ \frac{\mathcal{H}_{re}}{k} \sin[k(\tau - \tau_{re})] + \cos[k(\tau - \tau_{re})] \right\}, \end{aligned} \quad (2.6)$$

and it is valid for $k\tau \gg 1$ when all the corresponding wavelengths are shorter than the Hubble radius. In the same approximation $G_k(\tau)$ is:

$$G_k(\tau) = \frac{e^{-ik\tau_{ex}}}{a} \sqrt{\frac{k}{2}} \mathcal{Q}_k(\tau_{ex}, \tau_{re}) \left(\frac{a_{re}}{a_{ex}} \right) \times \left\{ \frac{\mathcal{H}_{re}}{k} \cos[k(\tau - \tau_{re})] - \sin[k(\tau - \tau_{re})] \right\}. \quad (2.7)$$

Equations (2.6)–(2.7) are valid in the two concurrent limits $k\tau \gg 1$ and $a_{re} \gg a_{ex}$ but they are otherwise general since the expansion rates at τ_{ex} and τ_{re} have not been specified. In Eqs. (2.6)–(2.7) $\mathcal{Q}_k(\tau_{ex}, \tau_{re})$ denotes a complex amplitude defined as:

$$\mathcal{Q}_k(\tau_{re}, \tau_{ex}) = 1 - (ik + \mathcal{H}_{ex}) \int_{\tau_{ex}}^{\tau_{re}} \frac{a_{ex}^2}{a^2(\tau)} d\tau. \quad (2.8)$$

The integral at the right hand side of Eq. (2.8) depends on the evolution between τ_{ex} and τ_{re} but its value is always subleading so that it is generally true⁴ that $|\mathcal{Q}_k(\tau_{re}, \tau_{ex})|^2 \rightarrow 1$.

In Eqs. (2.6)–(2.7) we may note the appearance of standing waves that are characteristic both in the case of relic gravitons and in the case of scalar metric fluctuations and they are often referred to as Sakharov oscillations because they arose, for the first time, in the pioneering contribution of Refs. [47, 48] (see also [49]). When Eqs. (2.6)–(2.7) are inserted into Eq. (2.2) we can obtain the corresponding power spectra that determine the final expression of the spectral energy density in critical units through Eq. (2.1):

$$\Omega_{gw}(k, \tau) = \frac{k^4}{12\pi^2 a^4 H^2 \bar{M}_p^2} |\mathcal{Q}(\tau_{ex}, \tau_{re})|^2 \times \left(\frac{a_{re}}{a_{ex}} \right)^2 \left(1 + \frac{\mathcal{H}_{re}^2}{k^2} \right) \left[1 + \mathcal{O}\left(\frac{\mathcal{H}}{k}\right) \right]. \quad (2.9)$$

Equation (2.9) is valid in the limit $\mathcal{H}/k \ll 1$ and this condition is equivalent to $k\tau \gg 1$ since $\mathcal{H} = \mathcal{O}(\tau^{-1})$. If a given wavelength exits the Hubble radius during inflation we have:

$$k \simeq a_{ex} H_{ex} \simeq -\frac{1}{(1-\epsilon)\tau_{ex}} = -\frac{\beta}{\tau_{ex}}, \quad (2.10)$$

where we denoted, for the sake of convenience, $\beta = 1/(1-\epsilon)$ and $\epsilon_{ex} = \epsilon \ll 1$. When the same wavelength reenters during a stage that is *not* dominated by radiation, $\epsilon_{re} \neq 2$ in Eq. (2.4) so that, at reentry, $k \simeq \mathcal{H}_{re} = a_{re} H_{re}$.

If a given wavelength $2\pi/k$ reenters across two different regimes characterized by a different expansion rate, the scale factor during the i -th stage of expansion can be parametrized, for instance, as:

$$a_i(\tau) = \left(\frac{\tau}{\tau_i} \right)^{\delta_i}, \quad \delta_i > 0, \quad \delta_i \neq 1, \quad \tau \leq \tau_i. \quad (2.11)$$

⁴ Only if $a^2(\tau) \simeq 1/\mathcal{H}$ the contribution of the integral of Eq. (2.8) is relevant and it corresponds to the possibility of extended stiff phases where, for instance, the energy density is dominated by the kinetic energy of a scalar field [31, 32]; in this case the spectral energy density and the other observables inherit a logarithmic correction.

For $\tau > \tau_i$ the scale factor during the $(i+1)$ -th stage of expansion is: modified as

$$a_{i+1}(\tau) \simeq \left[\frac{\delta_i}{\delta_{i+1}} \left(\frac{\tau}{\tau_i} - 1 \right) + 1 \right]^{\delta_{i+1}}, \quad \delta_{i+1} > 0, \quad \delta_{i+1} \neq 1, \quad \tau \geq \tau_i. \quad (2.12)$$

Even if δ_{i+1} and δ_i can be equal, the situation we want to discuss now is the one where $\delta_{i+1} \neq \delta_i$. Let us then go back to Eq. (2.9) and evaluate the spectral energy density for the modes reentering for $\tau < \tau_i$

$$\Omega_{gw}^{(i)}(k, \tau) = \frac{4}{3\pi} \left(\frac{H_1}{M_P} \right)^2 \left(\frac{H_1 a_1^2}{H a^2} \right)^2 \times \left| \frac{a_i H_i}{a_1 H_1} \right|^{4-\beta} \left| \frac{k}{a_i H_i} \right|^{n_T^{(i)}}, \quad k > a_i H_i, \quad (2.13)$$

where we took into account that $k \simeq a_{re} H_{re} = \mathcal{H}_{re}$. In Eq. (2.13) H_1 is coincides with the maximal value of the Hubble rate (e.g. at the end of inflation). We stress that, in the case $\epsilon_{re} \neq 2$, the turning points of Eq. (2.4) are determined from $k^2 \simeq a^2 H^2$; the contribution of the numerical factor $(2-\epsilon_{ex})$ and $(2-\epsilon_{re})$ has been consistently neglected. The spectral index appearing in Eq. (2.13) is given by

$$n_T^{(i)} = 2(1-\beta) + 2(1-\delta_i), \quad \delta_i > 0, \quad \beta = \frac{1}{1-\epsilon}. \quad (2.14)$$

If we now assume the validity of the consistency relations the value of $n_T^{(i)}$ depends on δ_i and r_T

$$n_T^{(i)}(r_T, \delta_i) = \frac{32-4r_T}{16-r_T} - 2\delta_i = 2(1-\delta_i) + \mathcal{O}(r_T). \quad (2.15)$$

From Eq. (2.15) in the limit $\delta_i \rightarrow 1$ we have

$$\lim_{\delta_i \rightarrow 1} n_T^{(i)}(r_T, \delta_i) = -r_T/8 + \mathcal{O}(r_T^2). \quad (2.16)$$

Similarly, for the wavelengths reentering during the $(i+1)$ -th stage the spectral energy density is instead given by:

$$\Omega_{gw}^{(i+1)}(k, \tau) = \frac{4}{3\pi} \left(\frac{H_1}{M_P} \right)^2 \left(\frac{H_1 a_1^2}{H a^2} \right)^2 \times \left| \frac{a_i H_i}{a_1 H_1} \right|^{4-\beta} \left| \frac{k}{a_i H_i} \right|^{n_T^{(i+1)}}, \quad k < a_i H_i, \quad (2.17)$$

where $n_T^{(i+1)}$ is now given by

$$n_T^{(i+1)}(r_T, \delta_{i+1}) = 2(1-\beta) + 2(1-\delta_{i+1}) = \frac{32-4r_T}{16-r_T} - 2\delta_{i+1} = 2(1-\delta_{i+1}) + \mathcal{O}(r_T). \quad (2.18)$$

From Eqs. (2.15)–(2.18) we have in fact three complementary possibilities. If the expansion rate is initially slower than radiation (i.e. $\delta_i < 1$) the spectral index for $k > a_i H_i$ is either blue or violet (i.e. $n_T^{(i)} > 0$). Then, provided $\delta_{i+1} > 1$ the spectral energy density of Eqs. (2.13) and (2.17) is characterized by a local minimum for $k \simeq a_i H_i$. We may also have the opposite situation where the expansion rate is initially faster than radiation (i.e. $\delta_i > 1$) then it gets smaller (i.e. $\delta_{i+1} < 1$) and the spectral energy density has a local maximum always for $k \simeq a_i H_i$. The third possibility suggests that either $\delta_i \rightarrow 1$ or $\delta_{i+1} \rightarrow 1$: in this case the spectral energy density exhibits a quasi-flat branch either for $\nu < \nu_i = a_i H_i$ or for $\nu > \nu_i$. While this result is formally correct, for the sake of completeness it is useful to verify it directly from Eq. (2.9). In the case $\delta_i \rightarrow 1$ at reentry we have that $k\tau_{re} \ll 1$; this means that the term $\mathcal{H}_{re}/k \gg 1$ dominates in Eq. (2.9) and $\Omega_{gw}(k, \tau)$ is then given by:

$$\begin{aligned}\Omega_{gw}(k, \tau) &= \frac{2}{3\pi} \left(\frac{k^2}{a_{ex}^2 M_P^2} \right) \left(\frac{H_{re}^2 a_{re}^4}{H^2 a^4} \right) \\ &= \frac{2}{3\pi} \left(\frac{H_1^2 a_1^4}{H^2 a^4} \right) \left(\frac{H_1}{M_P} \right)^2 \left(\frac{k}{a_1 H_1} \right)^{\bar{n}_T}, \quad (2.19)\end{aligned}$$

where $\bar{n}_T = -2\epsilon \simeq -r_T/8$. Thus Eqs. (2.16) and (2.19) show that $n_T^{(i)}(r_T, \delta_i)$ evaluated in the limit $\delta_i \rightarrow 1$ indeed corresponds to \bar{n}_T up to corrections $\mathcal{O}(r_T^2)$.

3 Peaks and troughs of the spectral energy density

The previous results demonstrate that \mathcal{H}_{re} and \mathcal{H}_{ex} are equally essential for the late-time form of the spectral energy density. In this sense the slopes of the humps appearing in $\Omega_{gw}(\nu, \tau_0)$ are a simultaneous test of the expansion rate during inflation and in the post-inflationary stage. This means that if $n_T^{(i)}(r_T, \delta_i)$ and $n_T^{(i+1)}(r_T, \delta_{i+1})$ are observationally assessed around a given peak, their measurement ultimately reflects the expansion history during and after inflation.

3.1 The profile of the effective expansion rate

It is now interesting to consider the general case illustrated in Fig. 1 where, prior to a_1 , an inflationary stage dominates the evolution of the background so that the effective expansion rate aH increases linearly with the scale factor. As suggested in the previous section, during this stage the initial inhomogeneities of the tensor modes are normalized to their quantum mechanical values. While in the conventional case we would have that, after inflation, the effective expansion rate is immediately dominated by radiation, in the situation illustrated in Fig. 1 we rather consider a sequence of different stages expanding either faster or slower than radiation.

More specifically, according to Fig. 1, the post-inflationary expansion history consists of N successive stages where, by definition, a_1 coincides with the end of inflation. Moreover, since a_r denotes the value of the scale factor at the onset of the radiation-dominated stage of expansion, we conventionally posit that $a_N = a_r$. During each of the successive stages the expansion rate is characterized, in the conformal time coordinate, by $a(\tau) \sim \tau^{\delta_i}$ so that the spectral index of $h_0^2 \Omega_{gw}(\nu, \tau_0)$ is in fact the one already determined in Eqs. (2.15) and (2.18). During the i -th stage of expansion the spectral energy density in critical units scales approximately as $(\nu/\nu_i)^{n_T^{(i)}}$. The dashed lines of Fig. 1 illustrate the values of the comoving frequencies at the transition points. Since the current value of the scale factor is conventionally normalized to 1 (i.e. $a_0 = 1$) comoving and physical frequencies coincide at the present time but not earlier on. Furthermore the largest frequency coincides with $a_1 H_1$ while for $\nu < \nu_r = a_r H_r$ the spectral energy density has the standard quasi-flat form since the corresponding wavelengths exit the Hubble radius during inflation and reenter when the Universe is already dominated by radiation. It is important to appreciate that while $\nu_1 = a_1 H_1 = \nu_{max}$ depends on all the post-inflationary expansion rates (i.e. the different δ_i), $\nu_r = a_r H_r$ only depends on the hierarchy between H_1 and H_r . To prove this statement it is practical to introduce the ratios of the curvature scales during two successive stages of expansion, namely:

$$\xi_i = \frac{H_{i+1}}{H_i} < 1, \quad \xi = \prod_i^{N-1} \xi_i = \frac{H_r}{H_1} < 1, \quad (3.1)$$

where ξ denotes the ratio between the Hubble rates at the onset of the radiation-dominated stage⁵ (i.e. H_r) and at the end of the inflationary phase (i.e. H_1); ξ_i gives instead the ratio of the expansion rates between two successive stages. Note that, by definition, both ξ_i and ξ are smaller than 1 since the largest value of the Hubble rate always appears in the denominator. Since we conventionally choose that H_1 coincides with the expansion rate at the end of inflation (i.e. $H_1 \equiv H_{max}$) while $H_N \equiv H_r$, in the simplest non-trivial situation we have that $N = 3$ and Eq. (3.1) implies:

$$\xi = \xi_1 \xi_2 = \frac{H_r}{H_1}, \quad \xi_1 = \frac{H_2}{H_1}, \quad \xi_2 = \frac{H_r}{H_2}, \quad (3.2)$$

where, following the conventions established established above and illustrated in Fig. 1, $a_3 = a_r$ and $H_3 = H_r$.

⁵ A curvature scale $H_r = \mathcal{O}(10^{-44}) M_P$ correspond to a temperature of the plasma $T = \mathcal{O}(\text{MeV})$. For the present ends it is more practical to work directly with the curvature scales.

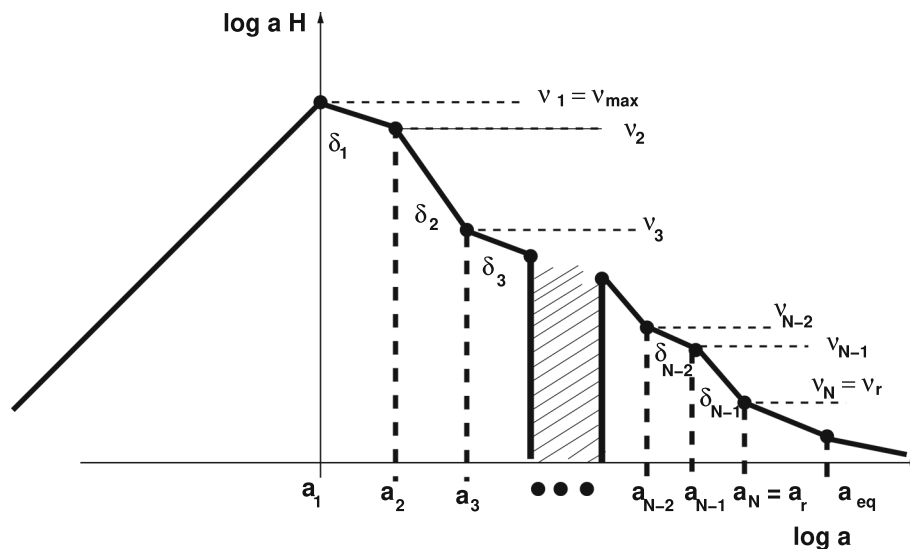


Fig. 1 On the vertical axis the common logarithm of aH is illustrated as a function of the common logarithm of the scale factor. We consider here the general situation where there are N different stages of expansion not necessarily coinciding with radiation. The N -th stage conventionally coincides with the standard radiation-dominated evolution (i.e. $a_r = a_N$) while the first stage starts at the end of inflation

(i.e. $H_1 = H_{\max}$). Even if, in general, $H_r \ll H_1$ we shall always require $H_r > 10^{-44} M_P$ implying that the dominance of radiation takes place well before big-bang nucleosynthesis. During the i -th stage of the sequence the scale factor expands as $a(\tau) \simeq \tau^{\delta_i}$. The dashed lines appearing in this cartoon correspond to the pivotal frequencies of the spectrum

3.2 The typical frequencies of the spectrum

As anticipated the maximal frequency of the spectrum indeed depends upon all the successive stages of expansion and its the general expression is:

$$v_1 = v_{\max} = \prod_{i=1}^{N-1} \xi_i^{\frac{\delta_i-1}{2(\delta_i+1)}} \bar{v}_{\max}. \quad (3.3)$$

In Eq. (3.3) \bar{v}_{\max} denotes the maximal frequency of the spectrum when all the different stages of expansion appearing in Fig. 1 collapse to a single phase expanding exactly like radiation. Indeed, if $\delta_i \rightarrow 1$ in Eq. (3.3) for all the $i = 1, \dots, N$ we have that $v_1 = v_{\max} \rightarrow \bar{v}_{\max}$:

$$\bar{v}_{\max} = 269.33 \left(\frac{r_T}{0.06} \right)^{1/4} \left(\frac{\mathcal{A}_{\mathcal{R}}}{2.41 \times 10^{-9}} \right)^{1/4} \left(\frac{h_0^2 \Omega_{R0}}{4.15 \times 10^{-5}} \right)^{1/4} \text{ MHz}, \quad (3.4)$$

where Ω_{R0} is the present fraction of relativistic species of the concordance scenario and $\mathcal{A}_{\mathcal{R}}$ is the amplitude of the scalar power spectrum that determines⁶ H_1 . In other words \bar{v}_{\max} coincides with the maximal frequency of the spectrum in the case considered in Refs. [5,6] where $H_1 \rightarrow H_r$ and $v_r \rightarrow v_{\max} = \mathcal{O}(200)$ MHz. In the general case illustrated

in Fig. 1 we have that:

$$v_N = v_r = \prod_{j=1}^{N-1} \sqrt{\xi_j} \bar{v}_{\max} = \sqrt{\xi} \bar{v}_{\max}, \quad (3.5)$$

where the second equality follows since, by definition,

$$\prod_{j=1}^{N-1} \xi_j = \xi_1 \xi_2 \cdots \xi_{N-2} \xi_{N-1} = \xi. \quad (3.6)$$

Equations (3.3) and (3.5) demonstrate, as anticipated above, that while v_{\max} is sensitive to the whole expansion history, v_r only depends upon $\sqrt{\xi}$ (where $\xi = H_r/H_1$).

For all the other intermediate frequencies between v_{\max} and v_r , the following expression holds:

$$v_m = \prod_{j=1}^{m-1} \sqrt{\xi_j} \prod_{i=m}^{N-1} \xi_i^{\frac{\delta_i-1}{2(\delta_i+1)}} \bar{v}_{\max}, \quad m = 2, 3, \dots, N-2, N-1. \quad (3.7)$$

The different frequencies are illustrated in Fig. 1 with the dashed lines are therefore in the following hierarchy:

$$v_{\max} = v_1 > v_2 > v_3 > \cdots > v_{N-2} > v_{N-1} > v_N = v_r. \quad (3.8)$$

The result of Eq. (3.8) is a direct consequence of the monotonic shape of aH for $a > a_1$. If the profile of aH is not monotonic for $a > a_1$, the hierarchy between the different frequencies of the spectrum is different as it happens when there is a second inflationary stage of expansion between a_1 and a_r [42].

⁶ We recall that $(H_1/M_P) = \sqrt{\pi \epsilon \mathcal{A}_{\mathcal{R}}}$. If the consistency relations are enforced we also have that $(H_1/M_P) = \sqrt{\pi r_T \mathcal{A}_{\mathcal{R}}}/4$, where $r_T \simeq 16\epsilon$ is, as usual, the tensor to scalar ratio.

3.3 Local maxima of the spectral energy density

Since the typical frequencies probed by space-borne interferometers are below the Hz the most interesting situation, from the practical viewpoint, involves a maximum of $h_0^2 \Omega_{gw}(\nu, \tau_0)$ just before the final dominance of radiation when $a_N = a_r$. In this case the extremum of the spectral energy density occurs for ν_{N-1} . Further maxima can also arise for higher frequencies and are more constrained by the measurements of the pulsar timing arrays and by the limits coming from wide-band detectors. Recalling the notations of Fig. 1 together with the explicit expressions of the slopes given in Eqs. (2.15) and (2.18), the spectral energy density has a maximum for $\nu = \nu_{N-1}$ provided

$$\begin{aligned} \delta_{N-2} \geq 1, \quad \delta_{N-1} < 1 \quad \Rightarrow \quad n_T^{(N-2)} \leq 0, \\ n_T^{(N-1)} > 0, \end{aligned} \quad (3.9)$$

where $\nu_{N-2} > \nu_{N-1} > \nu_N = \nu_r$. The spectral energy density in critical units reaches therefore a maximum for $\nu = \nu_{N-1}$ and its value is:

$$h_0^2 \Omega_{gw} = \bar{\mathcal{N}}_\rho(\nu_{N-1}, r_T) \left(\frac{\nu_{N-1}}{\nu_N} \right)^{n_T^{(N-1)}}. \quad (3.10)$$

where $\bar{\mathcal{N}}_\rho(\nu, r_T)$ is a function that weakly depends on the frequency and it is typically smaller than 10^{-16} for $r_T \leq 0.06$ [13–15]. This function is explicitly determined in Sect. 5 and it contains the dependence upon the transfer functions of the problem. According to the results deduced so far the explicit form of ν_{N-1} and ν_N is given by:

$$\nu_{N-1} = \sqrt{\xi_1} \dots \sqrt{\xi_{N-2}} \xi_{N-1}^{\frac{\delta_{N-1}-1}{2(\delta_{N-1}+1)}} \bar{\nu}_{max}, \quad (3.11)$$

$$\nu_N = \nu_r = \sqrt{\xi_1} \dots \sqrt{\xi_{N-1}} \bar{\nu}_{max}. \quad (3.12)$$

The ratio of Eqs. (3.11) and (3.12) gives exactly the term appearing in Eq. (3.10) so that the value of the spectral energy density at the maximum can also be written as:

$$h_0^2 \Omega_{gw}(\nu_{N-1}, \tau_0) \simeq \bar{\mathcal{N}}_\rho(\nu_{N-1}, r_T) \xi_{N-1}^{-\frac{2(1-\delta_{N-1})}{\delta_{N-1}+1}}. \quad (3.13)$$

The function $\bar{\mathcal{N}}_\rho(\nu_{N-1}, r_T)$ is weakly dependent on the frequency and its explicit form is discussed in the following section. Since the local maximum for $\nu = \nu_{N-1}$ does not depend on different maxima possibly arising for $\nu < \nu_{N-1}$ the simplest situation, for the present purposes, is the one where $N = 3$. In this case there are only two successive stages characterized by δ_1 and δ_2 . The maximal frequency of the spectrum is given by:

$$\nu_1 = \nu_{max} = \xi_1^{\frac{\delta_1-1}{2(\delta_1+1)}} \xi_2^{\frac{\delta_2-1}{2(\delta_2+1)}} \bar{\nu}_{max}. \quad (3.14)$$

The frequencies ν_2 and $\nu_3 = \nu_r$ are instead given by:

$$\begin{aligned} \nu_2 &= \sqrt{\xi_1} \xi_2^{\frac{\delta_2-1}{2(\delta_2+1)}} \bar{\nu}_{max}, \\ \nu_r &= \nu_3 = \sqrt{\xi_1} \sqrt{\xi_2} \bar{\nu}_{max}. \end{aligned} \quad (3.15)$$

We have just have one peak for $\nu = \nu_2$ and Eq. (3.13) gives

$$h_0^2 \Omega_{gw}(\nu_2, \tau_0) \simeq \bar{\mathcal{N}}_\rho(\nu_2, r_T) \xi_2^{-\frac{2(1-\delta_2)}{\delta_2+1}}. \quad (3.16)$$

All in all, while the existence of an early stage of accelerated expansion is motivated by general requirements directly related to causality, the post-inflationary expansion history is not constrained prior to big-bang nucleosynthesis. The results obtained in this section are therefore applicable to any post-inflationary expansion rate and do not assume the dominance of radiation between H_1 and H_r .

3.4 General requirements on the total number of e -folds

As repeatedly stressed we always considered hereunder the possibility that $H_r > 10^{-44} M_P$ suggesting that the plasma is already dominated by radiation for temperatures that are well above the MeV as it happens, for instance, when the reheating stage is triggered by the decay of a gravitationally coupled massive scalar field. There are however some possibilities where the MeV-scale reheating temperature could be induced by long-lived massive species with masses close to the weak scale, as suggested in Refs. [50, 51]. In spite of this interesting option we simply regard the condition $H_r \geq 10^{-44} M_P$ as an absolute lower limit on H_r . Indeed the gravitational waves only couple to the expansion rate and our purpose here is just to propose a framework where the early thermal history of the plasma could be tested via the spectra of the inflationary gravitons.

Along this perspective it is useful to remark that the maximal number of inflationary e -folds accessible to large-scale observations can be different [31] (see also [40, 42, 52]) depending on the post-inflationary expansion history. The maximal number of e -folds presently accessible to large-scale observation (\mathcal{N}_{max} in what follows) is computed by fitting the (redshifted) inflationary event horizon inside the current Hubble patch; in other words we are led to require, in terms of Fig. 1, that $H_1^{-1}(a_0/a_1) \simeq H_0^{-1}$. It is clear that \mathcal{N}_{max} does not coincide with the total number of e -folds that can easily be larger (or even much larger) than \mathcal{N}_{max} . Depending on the various δ_i and ξ_i the same gap in aH is covered by a different amount of redshift. In the general situation of Fig. 1 the expression of \mathcal{N}_{max} is given by:

$$\begin{aligned} \mathcal{N}_{max} &= 61.88 - \ln \left(\frac{h_0}{0.7} \right) + \frac{1}{4} \ln \left(\frac{r_T}{0.06} \right) + \frac{1}{4} \ln \left(\frac{\mathcal{A}_R}{0.06} \right) \\ &+ \frac{1}{4} \ln \left(\frac{h_0^2 \Omega_{R0}}{0.06} \right) + \frac{1}{2} \sum_i^{N-1} \left(\frac{\delta_i - 1}{\delta_i + 1} \right) \ln \xi_i. \end{aligned} \quad (3.17)$$

In connection with Eq. (3.17) we have three complementary possibilities. If we conventionally set $\delta_i = 1$ into Eq. (3.17) we obtain the standard result implying that $\mathcal{N}_{max} = \mathcal{O}(60)$. Recalling that all the ξ_i are, by definition, all smaller than 1 we have that $\mathcal{N}_{max} > 60$ if $\delta_i < 1$. For the same reason $\mathcal{N}_{max} < 60$ iff $\delta_i > 1$. Let us consider, for instance, the case of a single phase expanding slower than radiation; in this case \mathcal{N}_{max} can be as large as 75 [40,41]. In the intermediate situations where there are different phases expanding either faster or slower than radiation \mathcal{N}_{max} depends on the relative duration of the various phases and on their expansion rates.

4 The frequency range of space-borne interferometers

4.1 Approximate frequencies of the various instruments

While various space-borne interferometers have been proposed so far the presumed sensitivity of these instruments is still under debate. For this reason we adopt here a pragmatic viewpoint based on the considerations developed after Eq. (1.1). In short the strategy is the following:

- the fiducial frequency interval of space-borne interferometers ranges from a fraction of the mHz to the Hz and, within this interval, the minimal detectable spectral energy density (denoted hereunder by $h_0^2 \Omega_{gw}^{(min)}(\nu, \tau_0)$) defines the potential sensitivity of the hypothetical instrument;
- the LISA interferometers [21,22] might hopefully probe the following region of the parameter space:

$$h_0^2 \Omega_{gw}^{(min)}(\nu, \tau_0) = \mathcal{O}(10^{-11.2}),$$

$$10^{-4} \text{ Hz} < \nu \leq 0.1 \text{ Hz}; \quad (4.1)$$

- in the case of the Deci-Hertz Interferometer Gravitational Wave Observatory (DECIGO) [23,24] the minimal detectable spectral energy density could be smaller

$$10^{-17.5} \leq h_0^2 \Omega_{gw}^{(min)}(\nu, \tau_0) \leq \mathcal{O}(10^{-13.1}),$$

$$10^{-3} \text{ Hz} < \nu \leq 0.1 \text{ Hz}. \quad (4.2)$$

The values of Eq. (4.2) are still quite hypothetical so that it is prudent to choose $h_0^2 \Omega_{gw}^{(min)}(\nu, \tau_0)$ between the standard values of the hoped sensitivity of the DECIGO project [23,24] (suggesting $h_0^2 \Omega_{gw}^{(min)}(\nu, \tau_0) = \mathcal{O}(10^{-13.1})$) and the optimistic figure reachable by the Ultimate-DECIGO [25] (conventionally referred to as U-DECIGO) where $h_0^2 \Omega_{gw}^{(min)}(\nu, \tau_0) = \mathcal{O}(10^{-17.5})$. For the record, the Big Bang Observer (BBO) [26] might reach sensitivities

$$h_0^2 \Omega_{gw}^{(min)}(\nu, \tau_0) = \mathcal{O}(10^{-14.2}), \quad 10^{-3} \text{ Hz} < \nu \leq 0.1 \text{ Hz}. \quad (4.3)$$

There finally exist also recent proposals such as Taiji [27,28] and TianQin [29,30] leading to figures that are roughly comparable with the LISA values. In summary for the typical frequency of the space-borne detectors we consider the following broad range:

$$0.1 \text{ mHz} < \nu_S < 0.1 \text{ Hz} \quad (4.4)$$

and suppose that in the range (4.4) $h_0^2 \Omega_{gw}^{(min)}(\nu, \tau_0)$ may take the following two extreme values.

$$h_0^2 \Omega_{gw}^{(min)}(\nu_S, \tau_0) = \mathcal{O}(10^{-11}),$$

$$h_0^2 \Omega_{gw}^{(min)}(\nu_S, \tau_0) = \mathcal{O}(10^{-14}). \quad (4.5)$$

While the two values of Eq. (4.5) are both quite optimistic, they are customarily assumed by the observational proposals and, for this reason, they are used here only for illustration.

4.2 The profile of the spectral energy density

The exclusion plots characterizing the parameter space of the model are separately considered for the two illustrative values of $h_0^2 \Omega_{gw}^{(min)}(\nu_S, \tau_0)$ given in Eq. (4.5). For instance in Fig. 2 we require that

$$\nu_{N-1} = \mathcal{O}(\nu_S), \quad h_0^2 \Omega_{gw}(\nu_{N-1}, \tau_0) \geq 10^{-11}. \quad (4.6)$$

The first requirement of Eq. (4.6) implies that the frequency range of the maximum is comparable with ν_S while the second condition just comes from Eq. (4.5) and it also demands, incidentally, that the inflationary signal is larger than the spectral energy density produced by the gravitational waves associated with a putative strongly first-order phase transition, as we shall briefly discuss later on. The condition (4.6) can also be relaxed by assuming the second value of $h_0^2 \Omega_{gw}(\nu_S, \tau_0)$:

$$\nu_{N-1} = \mathcal{O}(\nu_S), \quad h_0^2 \Omega_{gw}(\nu_{N-1}, \tau_0) \geq 10^{-14}. \quad (4.7)$$

Equation (4.7) is justified by the nominal sensitivity of other space-borne interferometers such as DECIGO [23,24] or U-DECIGO [25]. To investigate the phenomenological implications the simplest choice is to posit $N = 3$. In this case we just have one maximum for $\nu_r < \nu < \nu_{max}$ and the discussion of the parameters is therefore simpler even if, as already mentioned, the essential features remain the same also in more complicated situations. For $N = 3$ the spectral energy density of the model is:

$$h_0^2 \Omega_{gw}(\nu, \tau_0) = \mathcal{N}_\rho r_T(\nu_p) \left(\frac{\nu}{\nu_p} \right)^{\bar{n}_T(r_T)} \times \mathcal{T}_{low}^2(\nu/\nu_{eq}) \mathcal{T}_{high}^2(\nu, \nu_2, \nu_r, n_T^{(1)}, n_T^{(2)}), \quad (4.8)$$

where $\bar{n}_T(r_T)$ has been computed in Eqs. (2.16) and (2.19); \bar{n}_T is the spectral index associated with the wavelengths leav-

ing the Hubble radius during the inflationary phase and reentering during the radiation stage. In Eq. (4.8) ν_p and ν_{eq} define the lowest frequency range of the spectral energy density:

$$\nu_p = \frac{k_p}{2\pi} = 3.092 \left(\frac{k_p}{0.002 \text{ Mpc}^{-1}} \right) \text{ aHz},$$

$$\nu_{eq} = \frac{k_{eq}}{2\pi} = 15.97 \left(\frac{h_0^2 \Omega_{M0}}{0.1411} \right) \left(\frac{h_0^2 \Omega_{R0}}{4.15 \times 10^{-5}} \right)^{-1/2} \text{ aHz}, \quad (4.9)$$

where we used that $k_{eq} = 0.0732 h_0^2 \Omega_{M0} \text{ Mpc}^{-1}$ (as usual, Ω_{M0} is the present fraction in dusty matter). The spectral slopes $n_T^{(1)}$ and $n_T^{(2)}$ are instead determined by Eqs. (2.15) and (2.18); up to corrections $\mathcal{O}(r_T)$ we have

$$n_T^{(1)} = 2(1 - \delta_1) + \mathcal{O}(r_T),$$

$$n_T^{(2)} = 2(1 - \delta_2) + \mathcal{O}(r_T), \quad (4.10)$$

where $n_T^{(1)} < 0$ and $n_T^{(2)} > 0$ since during the first stage the Universe expands faster than radiation (i.e. $\delta_1 > 1$) while in the second stage it is slower than radiation (i.e. $\delta_2 < 1$). In the simplest case where the consistency relations are enforced we have that

$$\bar{n}_T(r_T) = -\frac{r_T}{8} + \mathcal{O}(r_T^2),$$

$$\mathcal{N}_\rho = 4.165 \times 10^{-15} \left(\frac{h_0^2 \Omega_{R0}}{4.15 \times 10^{-5}} \right). \quad (4.11)$$

In Eq. (4.9) $\mathcal{T}_{low}(\nu/\nu_{eq})$ is the low-frequency transfer function of the spectral energy density [20]:

$$\mathcal{T}_{low}(\nu, \nu_{eq}) = \sqrt{1 + c_1 \left(\frac{\nu_{eq}}{\nu} \right) + c_2 \left(\frac{\nu_{eq}}{\nu} \right)^2},$$

$$c_1 = 0.5238, \quad c_2 = 0.3537. \quad (4.12)$$

The high-frequency transfer function $\mathcal{T}_{high}(\nu, \nu_2, \nu_r, \delta_1, \delta_2)$ appearing in Eq. (4.8) depends on ν_2 and ν_r and it is given by:

$$\mathcal{T}_{high}^2(\nu, \nu_r, \nu_2, n_T^{(1)}, n_T^{(2)}) = \frac{\sqrt{1 + b_1(\nu/\nu_r)^{n_T^{(2)}} + b_2(\nu/\nu_r)^{2n_T^{(2)}}}}{\sqrt{1 + d_1(\nu/\nu_2)^{n_T^{(2)} + |n_T^{(1)}|} + d_2(\nu/\nu_2)^{2(n_T^{(2)} + |n_T^{(1)}|)}}}, \quad (4.13)$$

where b_i and d_i (with $i = 1, 2$) are numerical coefficients of order 1 that depend on the specific choice of δ_1 and δ_2 and cannot be written in general terms. We recall that the explicit expressions of ν_2 and ν_r have been given in Eq. (3.15) and they depend explicitly upon ξ_1 and ξ_2 . Since Eq. (4.13) depends on *two different scales*, there are *three relevant limits* of $\mathcal{T}_{high}^2(\nu, \nu_r, \nu_2)$ that must be considered. The first limit stipulates that:

$$\mathcal{T}_{high}^2(\nu, \nu_r, \nu_2, n_T^{(1)}, n_T^{(2)}) \rightarrow \sqrt{\frac{b_2}{d_2}} \left(\frac{\nu_2}{\nu_r} \right)^{n_T^{(2)}} \left(\frac{\nu}{\nu_2} \right)^{-|n_T^{(1)}|}, \quad \nu \gg \nu_2, \quad (4.14)$$

and it corresponds to the high-frequency branch where the spectral energy density is suppressed as $\nu^{-|n_T^{(1)}|}$:

$$h_0^2 \Omega(\nu, \tau_0) = \bar{\mathcal{N}}_\rho(r_T, \nu) \left(\frac{\nu_2}{\nu_r} \right)^{n_T^{(2)}} \left(\frac{\nu}{\nu_2} \right)^{-|n_T^{(1)}|},$$

$$\nu_2 < \nu < \nu_{max}. \quad (4.15)$$

Note that since $n_T^{(1)} < 0$, in the spectral energy density we introduced the absolute value just to avoid potential confusions. This is not necessary in the case of $n_T^{(2)}$ which is instead positive semidefinite. From Eq. (4.13) the second relevant limit corresponds to the region where $\nu < \nu_2$:

$$\mathcal{T}_{high}^2(\nu, \nu_r, \nu_2, n_T^{(1)}, n_T^{(2)}) \rightarrow \sqrt{b_2} \left(\frac{\nu}{\nu_r} \right)^{n_T^{(2)}}, \quad \nu_r < \nu < \nu_2. \quad (4.16)$$

In this case the spectral energy density increases as $\nu^{n_T^{(2)}}$ and its approximate expression is given by:

$$h_0^2 \Omega(\nu, \tau_0) = \bar{\mathcal{N}}_\rho(r_T, \nu) \left(\frac{\nu}{\nu_r} \right)^{n_T^{(2)}}, \quad \nu_r < \nu < \nu_2. \quad (4.17)$$

The third relevant limit of the transfer function is finally for $\nu < \nu_r$ and, in this limit, Eq. (4.13) simply goes to 1:

$$\mathcal{T}_{high}^2(\nu, \nu_r, \nu_2, n_T^{(1)}, n_T^{(2)}) \rightarrow 1, \quad \nu < \nu_r. \quad (4.18)$$

The function $\bar{\mathcal{N}}_\rho(\nu, r_T)$ has been already introduced in Eq. (3.10) and, as anticipated, its explicit expression depends in fact upon the low-frequency transfer function:

$$\bar{\mathcal{N}}_\rho(r_T, \nu) = \mathcal{N}_\rho r_T \left(\frac{\nu}{\nu_p} \right)^{\bar{n}_T} \mathcal{T}_{low}^2(\nu_r/\nu_{eq}),$$

$$\frac{d \ln \bar{\mathcal{N}}_\rho}{d \ln \nu} = -\frac{r_T}{8} \ll 1. \quad (4.19)$$

Even though the prefactor $\bar{\mathcal{N}}_\rho(r_T, \nu)$ has a mild frequency dependence coming from neutrino free-streaming, for simplified analytic estimates this dependence can be ignored, at least approximately; this in fact the meaning of the second relation in Eq. (4.19). Along this perspective we can estimate $\bar{\mathcal{N}}_\rho = \mathcal{O}(10^{-16.5})$ for $r_T = 0.06$.

4.3 The constrained parameter space

The shaded region in Fig. 2 illustrates the area of the parameter space where the following pair of conditions are simultaneously verified:

$$h_0^2 \Omega_{gw}(\nu_2, \tau_0) \geq h_0^2 \Omega_{gw}^{(min)},$$

$$0.1 \text{ mHz} < \nu_2 \leq 0.1 \text{ Hz}. \quad (4.20)$$

Since the product of the various ξ_i from 1 to $(N - 1)$ must equal ξ , in the case of $N = 3$ we have that $\xi_1 \xi_2 = \xi$. Then the analysis can be simplified by using three related observations:

- ξ_1 can be traded for ξ/ξ_2 by recalling that, to avoid problems with nucleosynthesis, the lower limit $\xi > 10^{-38}$ must always be separately imposed;
- as a consequence we end-up with three parameters ξ_2 , ξ , δ_1 and δ_2 ;
- to discuss the parameter space we can fix $\delta_1 \rightarrow 1$: this is the most constraining value since for $\delta_1 > 1$ the high-frequency part of $h_0^2 \Omega_{gw}(\nu, \tau_0)$ decreases and it is therefore less constrained by the high-frequency limits.

If the spectral energy density decreases for $\nu > \nu_2$ (i.e. $n_T^{(1)} < 0$) all the high-frequency bounds (and in particular the LIGO-Virgo-KAGRA limit [18–20]) are automatically satisfied *provided* they are satisfied in the case $\delta_1 \rightarrow 1$. The value of δ_1 affects the value of the high-frequency slope of the spectral energy density since, in this case, $n_T^{(1)}(r_T, \delta_1) = \mathcal{O}(r_T)$.

In the four different plots of Fig. 2 the value of ξ increases from 10^{-36} to 10^{-30} so that the radiation dominates when the expansion rate gets progressively larger; recall, in fact, that $\xi = H_r/H_1 \geq 10^{-38}$. As ξ increases the duration of the radiation phase increases, the shaded area gets smaller and allowed region is reduced. The same logic of Fig. 2 has been followed in the case of Fig. 3 with the difference that $h_0^2 \Omega_{gw}^{(min)}$ is now relaxed from 10^{-11} to 10^{-14} . In each of the plots appearing in Figs. 2 and 3 there are two shaded regions. The wider area is obtained by enforcing the big-bang nucleosynthesis (BBN) constraint [53–55]. The narrower (and darker) region in each plot of Figs. 2 and 3 is instead obtained by imposing the limits obtained from the operating interferometers on the backgrounds of relic gravitons, i.e. the LIGO-Virgo-KAGRA bound [18] (see also [19, 20]).

From the technical viewpoint the BBN constraint requires⁷:

$$\begin{aligned} h_0^2 \int_{\nu_{bbn}}^{\nu_{max}} \Omega_{gw}(\nu, \tau_0) d \ln \nu \\ = 5.61 \times 10^{-6} \Delta N_\nu \left(\frac{h_0^2 \Omega_{\gamma 0}}{2.47 \times 10^{-5}} \right), \end{aligned} \quad (4.21)$$

where $\Omega_{\gamma 0}$ is the (present) critical fraction of CMB photons and ν_{bbn} denotes the BBN frequency:

$$\begin{aligned} \nu_{bbn} = 2.252 \times 10^{-11} \left(\frac{N_{eff}}{10.75} \right)^{1/4} \\ \times \left(\frac{T_{bbn}}{\text{MeV}} \right) \left(\frac{h_0^2 \Omega_{R0}}{4.15 \times 10^{-5}} \right)^{1/4} \text{ Hz}, \end{aligned} \quad (4.22)$$

where N_{eff} denotes the effective number of relativistic degrees of freedom entering the total energy density of the

plasma and T_{bbn} is the temperature of big-bang nucleosynthesis. The bound (4.22) can be relaxed if the nucleosynthesis takes place in the presence of matter-antimatter domains [54] and ν_{max} appearing in Eq. (4.21) denotes, as previously discussed, the maximal frequency of the spectrum. However, since $h_0^2 \Omega_{gw}(\nu, \tau_0)$ decreases for $\nu > \nu_2$ (and more generally for $\nu > \nu_{N-1}$) the region between ν_2 and ν_{max} gives a subleading contribution to the integral appearing at the left-hand side of Eq. (4.21).

According to Figs. 2 and 3 the limits imposed by Eqs. (4.21)–(4.22) are less constraining than the ones following from the LIGO-Virgo-KAGRA bound [18]. Indeed the LIGO-Virgo-KAGRA collaboration, in its attempt to constrain the stochastic backgrounds of relic gravitons, reported a constraint [18] implying, in the case of a quasi-flat spectral energy density in the audio-band

$$\Omega_{gw}(\nu, \tau_0) < 5.8 \times 10^{-9}, \quad 20 \text{ Hz} < \nu_{KLV} < 76.6 \text{ Hz}, \quad (4.23)$$

where ν_{LVK} denotes the LIGO-Virgo-KAGRA frequency. The exclusion plots of Fig. 2 are then confronted with the current phenomenological bounds in all the available ranges of frequency with the aim of constraining the rate and the duration post-inflationary expansion Universe. In particular, in the nHz region, the pulsar timing arrays (PTA) recently reported a potential signal that could be attributed to the relic gravitons [43–46]. The PTA recently reported evidence of a potential signal in the nHz band. Using the spectral energy density in critical units as a pivotal variable the features of this purported signal would imply, in the present notations, that:

$$\begin{aligned} q_0^2 \times 10^{-8.86} < h_0^2 \Omega_{gw}(\nu, \tau_0) < q_0^2 \times 10^{-9.88}, \\ 3 \text{ nHz} < \nu < 100 \text{ nHz}. \end{aligned} \quad (4.24)$$

In Eq. (4.24) we introduced the numerical factor q_0 that depends on the specific experimental determination. The Parkes Pulsar Timing Array collaboration [43] suggests $q_0 = 2.2$. Similarly the International Pulsar Timing Array collaboration (IPTA in what follows) estimates $q_0 = 2.8$ [44] while the European Pulsar Timing Array collaboration (EPTA in what follows) [45] gives $q_0 = 2.95$ (see also [56, 57]). The results of PPTA, IPTA and EPTA seem, at the moment, to be broadly compatible with the NANOgrav 12.5 years data [46] (see also [58, 59]) implying $q_0 = 1.92$.

It is relevant to point out that neither the observations of Refs. [43–45] nor the ones of Ref. [46] can be interpreted yet as an evidence of relic gravitons. The property of a PTA is that the signal from relic gravitons will be correlated across the baselines, while that from the other noise will not. Since these correlation have not been observed so far, the interpretation suggested in Eq. (4.24) is still preliminary, to say the least. To be fair the pragmatic strategy followed here will be

⁷ The limit of Eq. (4.22) sets a constraint on the extra-relativistic species possibly present at the BBN time. The limit is often expressed for practical reasons in terms of ΔN_ν representing the contribution of supplementary neutrino species. The actual bounds on ΔN_ν range from $\Delta N_\nu \leq 0.2$ to $\Delta N_\nu \leq 1$; the integrated spectral density in Eq. (4.22) is thus between 10^{-6} and 10^{-5} .

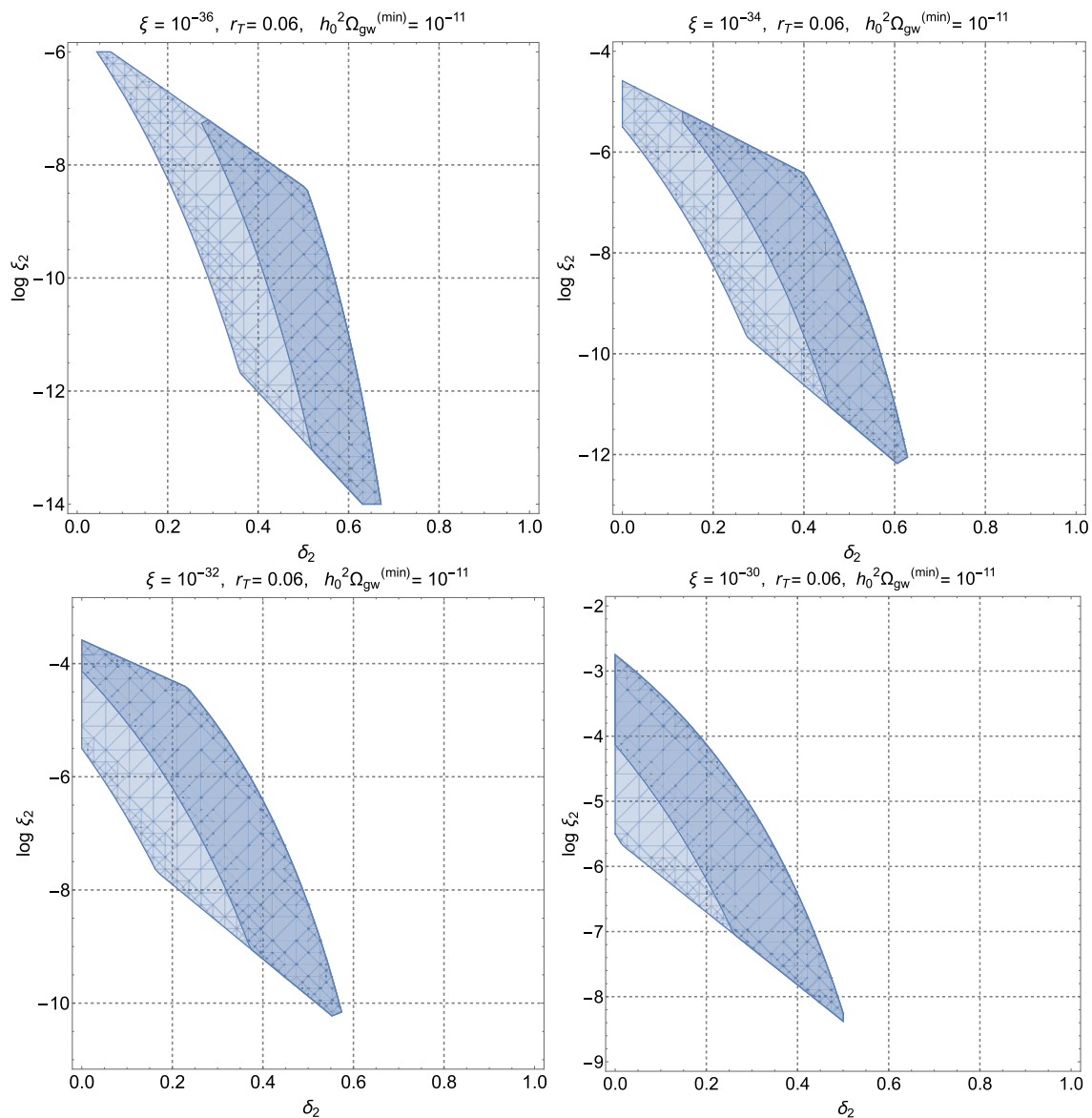


Fig. 2 The parameter space is illustrated in the plane (δ_2, ξ_2) by fixing δ_1 to its most constraining value realized in the case $\delta_1 \rightarrow 1$. In the four different plots of this figure the value of ξ progressively increases between 10^{-38} and 10^{-30} . The shaded area corresponds to the allow

region. The wider area is obtained by enforcing the big-bang nucleosynthesis limit of Eqs. (4.21)–(4.22) while the smaller (and darker) region follows by imposing the limits coming from the audio band (see Eqs. (4.23)) and discussion therein

to interpret Eq. (4.24) as an upper limit whenever the corresponding theoretical signal is too low in the nHz region. Conversely if $h_0^2 \Omega_{gw}(\nu, \tau_0)$ happens to be grossly compatible with the range of Eq. (4.24) it will be interesting to see if the associated spectral energy density fits within the PTA window. The average of the q_0 of the different experiments

is given by $\bar{q}_0 = 2.46$. If we use \bar{q}_0 into Eq. (4.24) we get to the requirement:

$$10^{-8.07} < h_0^2 \Omega_{gw}(\nu, \tau_0) < \times 10^{-9.09},$$

$$3 \text{ nHz} < \nu < 100 \text{ nHz}. \quad (4.25)$$

The condition (4.25) is never verified for the parameter space illustrated in Figs. 2 and 3. Thus, for the selection of param-

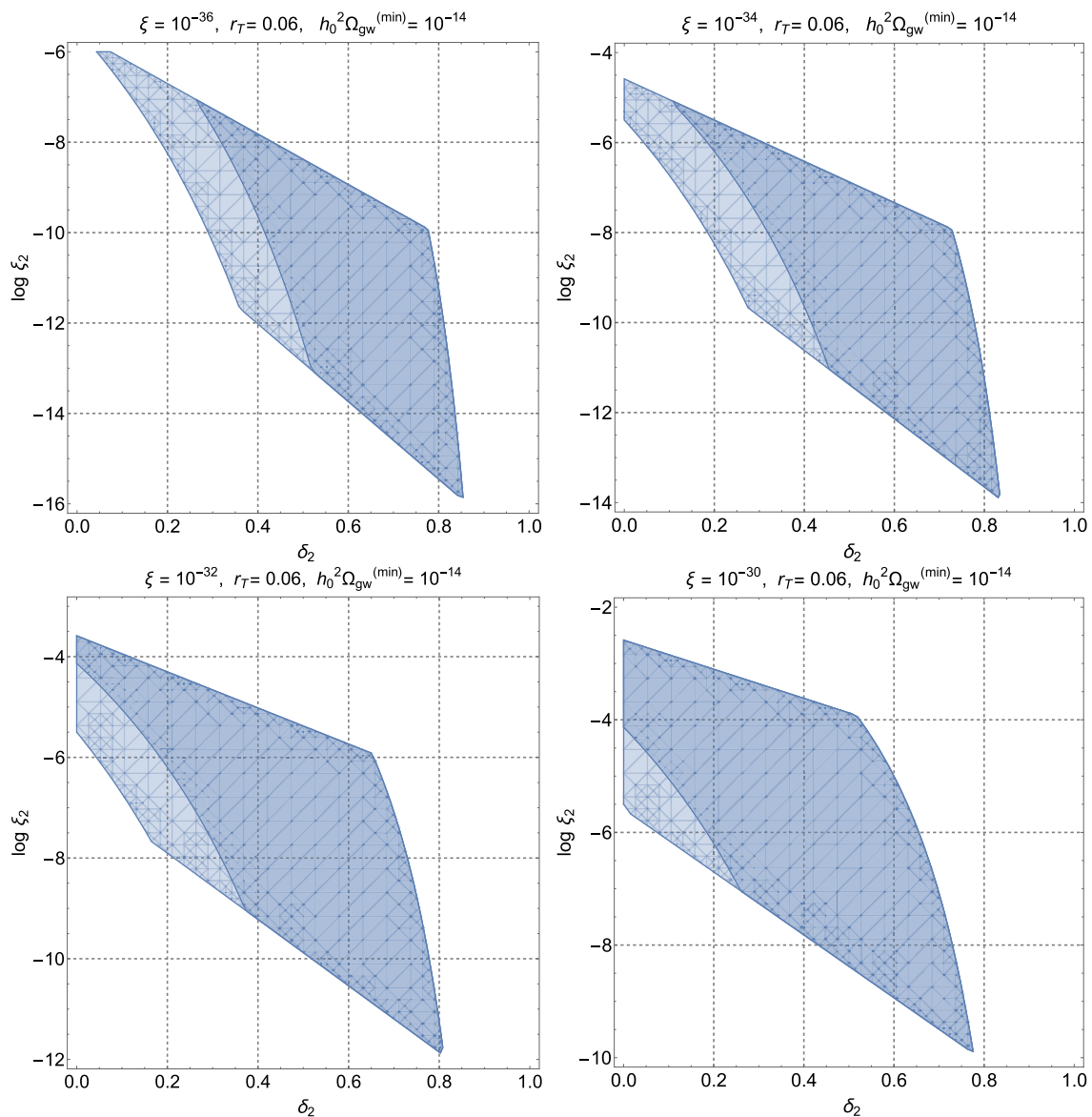


Fig. 3 As in Fig. 2 the parameter space of the model is illustrated in the plane (δ_2, ξ_2) . The difference between these plots and the ones of Fig. 2 is related to $h_0^2 \Omega_{gw}^{(min)}$ which is now given by 10^{-14} while it was 10^{-11} in Fig. 2

ters analyzed here, $h_0^2 \Omega_{gw}(\nu, \tau_0)$ may lead to a relevant signal below the Hz but not in the nHz band.

4.4 The spectral energy density and its signatures

In Figs. 4 and 5, the spectral energy density has been explicitly illustrated for a selection of the parameters. In Fig. 4 we selected $\xi = 10^{-36}$ and $\xi_2 = 10^{-10}$ for different values of $\delta_1 > 1$ and $\delta_2 < 1$. As expected the value of ν_r is always larger than 10^{-10} . For this reason $h_0^2 \Omega_{gw}(\nu, \tau_0)$ does not exceed $\mathcal{O}(10^{-16})$ in the frequency range of the PTA and the profiles of Figs. 4 and 5 are unable to account for the putative signal of Eqs. (4.24)–(4.25). Note, in this respect, that

the parameters of the dot-dashed and of the dashed curves of Fig. 4 have been selected in order to get an artificially large signal that is in fact excluded both by the constraint of Eq. (4.21) and by the limit of ground-based detectors (see Eq. (4.23) and discussion therein). Even in this case the PTA values are too large and must be accounted by different mechanisms. The results of Fig. 5 correspond instead to a slightly different choice of the parameters, namely $\xi = 10^{-34}$ and $\xi_2 = 10^{-8}$. For illustration we have chosen $\delta_1 \rightarrow 1$ implying that between ν_{max} and ν_2 the spectral energy density is quasi-flat. This is the most constraining case from the viewpoint of the limits coming from wide-band detectors [18–20].

Fig. 4 We illustrate the common logarithm of the spectral energy density of the relic gravitons as a function of the common logarithm of the frequency expressed in Hz. In this plot the dashed and the dot-dashed curves illustrate two models that are excluded by the big-bang nucleosynthesis constraint of Eq. (4.21) and by the LIGO-Virgo-KAGRA limit of Eq. (4.23). The parameters of the curve at the bottom (full line) are instead drawn from the allowed region of the parameter space. In all the examples of this plot $\delta_1 > 1$

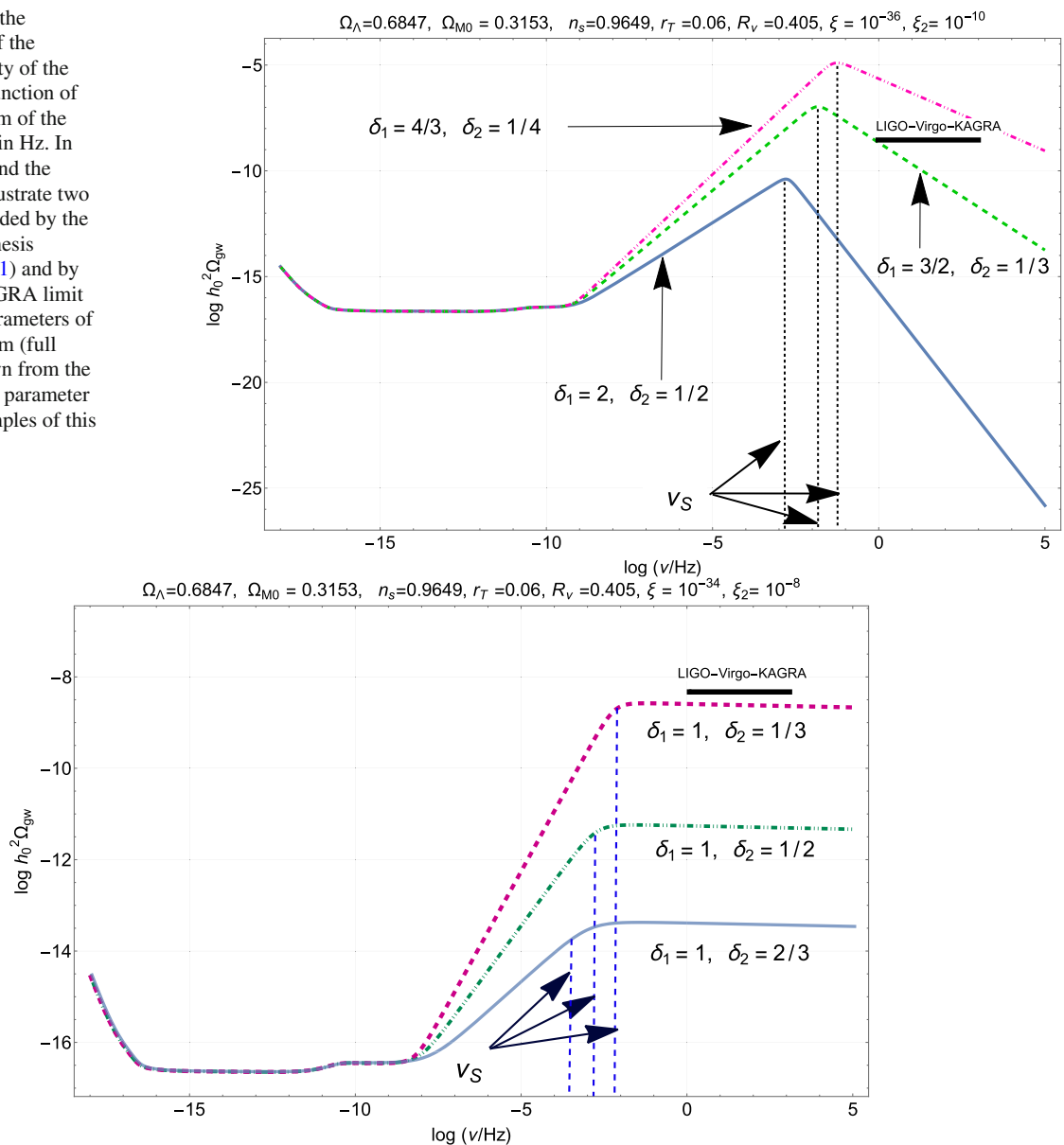


Fig. 5 The conventions are exactly the same already explained in Fig. 4 but the spectral energy is illustrated for a different choice of the parameters. The dashed curves at the top of the figure is barely compatible with the limits set by Eq. (4.23). If $\delta_1 > 1$ (see e.g. Fig. 4) the spectral energy density decreases for $\nu > \nu_2$ and the most relevant constraint on the

height of the maximum comes from Eqs. (4.21)–(4.22). If $\delta_1 \rightarrow 1$ the limits from the audio band (see, in particular, Eq. (4.23)) are the most constraining ones and this is why we illustrated here this case where the spectral energy density remains quasi-flat at high-frequencies

The class of signals computed here are distinguishable, at least in principle, from the other astrophysical and cosmological foregrounds. In the region between a fraction of the mHz and the Hz the predominant astrophysical foregrounds of gravitational radiation are probably associated with the galactic distribution of the white dwarves. While the signal of white dwarves could also be used for calibration, other astrophysical foregrounds are also expected (e.g. stellar origin black holes and even supermassive black holes

from galaxy mergers). Another cosmological foreground is given by TeV scale early Universe and this happens since the typical frequency corresponding to the Hubble radius at the electroweak stage is $\mathcal{O}(10) \mu\text{Hz}$. To have drastic deviations from homogeneity and the consequent production of burst of gravitational radiation the electroweak phase transition must be strongly first-order. In this respect two classes of related observations are in order. The first remark is that the electroweak phase transition does not have to be strongly

first-order. Since the first perturbative analyses of the problem we actually know that that for the measured range of Higgs masses the electroweak phase transition is not of first-order [60, 61]. Due to the inherently non-perturbative nature of the problem, the original perturbative estimates have been subsequently corroborated by lattice calculations both in three [62] and four dimensions [63]. For the measured values of the Higgs and gauge boson masses the transition between the symmetric and the broken phase follows a cross-over evolution that should not lead to an appreciable production of gravitational radiation. In this case the only cosmological signal may be the one associated with the inflationary gravitons.

The second remark is that, at the moment the hopes of observing a burst of gravitational radiation from the electroweak scale must rely on some extension of the standard electroweak theory. In this situation the amount of gravitational radiation produced by the phase transition depends on the particular model and also on the difference between the energy density in the broken and in the symmetric phase. This energy density may be comparable with the energy density of the ambient plasma (and in this case the phase transition experiences a strong supercooling) or smaller than the energy density of the surrounding radiation (and in this case the phase transition is mildly supercooled). If the gravitational is produced from the collisions of the bubbles of the new phase [64–66] the equivalent $h_0^2 \Omega_{gw}(\nu, \tau_0)$ scales like ν^3 , reaches a maximum and then decreases with a power that may be faster than ν^{-1} . The spectral energy density inherits also contribution from the sound waves of the plasma [67] and this second component may be even larger than the one due to bubble collisions. The key point for the present ends is that the powers associated with a strongly first-order phase transition are typically much steeper than the ones discussed here. In our case the rise of $h_0^2 \Omega_{gw}(\nu, \tau_0)$ appearing in Figs. 4 and 5 always scales with $0 < n_T^{(2)} \leq 1$ while the corresponding slope in the case of phase transitions is typically $\mathcal{O}(3)$. Another possibility not requiring a strongly first-order phase transition is the presence of a stochastic background of hypermagnetic fields at the electroweak phase. In this case bursts of gravitational radiation may also be produced and the spectral energy density is different from the one discussed here [68] (see also [69, 70]). Overall, because of causality, the spectra associated with the TeV physics are much steeper around their putative maximum. For this reason it seems plausible to disentangle the inflationary contributions from other possible cosmological foregrounds. There is of course a deeper problem that has to do with our ability to separate the cosmological signals from the other astrophysical foregrounds (e.g. white dwarves, massive and supermassive black-holes). The potential difficulties associated with the astrophysical foregrounds suggested already many years ago [31, 32] that the

potential signals of post-inflationary stages should be probably observed over much higher frequencies $\mathcal{O}(\text{MHz})$ where electromagnetic detectors might be operating in the future [71–77].

4.5 Complementary considerations

Even if specific scenarios involving high, intermediate and low reheating temperatures have been suggested in the past [31–33] (see also, in this respect, Refs. [34–42]), the present analysis focussed on a model-independent perspective. Given that the early expansion history of the background is unknown the only plausible strategy is to combine the low-frequency limits and of the high-frequency constraints. This approach suggests that a signal below the Hz is not excluded and the features of the spectra can be clearly distinguished from the ones of strongly first-order phase transitions that are the main competitive signal in this region. We might think, by the same token, that large signals can be achieved also over much smaller frequencies and it is then interesting to apply the present model-independent strategy in this instance.

By looking at Figs. 4 and 5 we may note that the first break from scale invariance of the spectral energy density always occurs above a typical frequency $\mathcal{O}(10^{-10})$ Hz. This feature persists if the number of successive stages of expansion is increased and the ultimate reason for this occurrence is given by Eqs. (3.5)–(3.6): while all the intermediate frequencies of the spectrum are given by a complicated combination involving the various expansion rates and the intermediate curvature scales (see e.g. Eqs. (3.7)–(3.8)) ν_r is solely determined by the ratio between H_r and H_1 . This means that the absolute lower limit $H_r \geq 10^{-44} M_P$ imposed by big-bang nucleosynthesis also implies that $\nu_r > \mathcal{O}(10^{-10})$ Hz, or, more precisely $\nu > \nu_{bbn}$. This requirement is essential when combining the high-frequency limits on the relic gravitons with the low-frequency one [40, 41] and it has been correctly implemented in a recent analysis focusing on the post-inflationary reheating parameters [79]. A direct consequence of this requirement is that the recent results of the PTA (see Eq. (4.25)) cannot be explained by a post-inflationary modification of the expansion rate. Given the current limits on r_T [13–15] the largest value of $h_0^2 \Omega_{gw}$ for $\nu < \nu_r$ is, at most, $\mathcal{O}(10^{-16.5})$. Since $\nu_r \geq \mathcal{O}(10^{-10})$ Hz it is impossible that $h_0^2 \Omega_{gw}$ reaches a value $\mathcal{O}(10^{-9})$ for typical frequencies of the order of 10 nHz or even 100 nHz as required for an explanation of the PTA observations [43–46]. We actually remind that the largest slope of the spectral energy density, in the case of a barotropic fluid, is of order 1 and it occurs for a nearly stiff equation of state, as established long ago [31, 32]. There have been nonetheless claims of a sound explanation of the PTA data by post-inflationary stiff phases. For instance

in Ref. [80] the authors just suggest the opposite of what we just said; by looking more carefully at the results⁸ we see that, in this case, $\nu_r = \mathcal{O}(10^{-14})$ Hz. By appealing to the model-independent results of Eqs. (3.5)–(3.6) that apply strictly also in this case we have therefore

$$\nu_r = \mathcal{O}(10^{-14}) \text{ Hz} \quad \Rightarrow \quad \xi = \mathcal{O}(10^{-45}), \quad (4.26)$$

and if we now recall that $\xi = H_r/H_1$ we conclude that

$$\frac{H_r}{M_P} = \mathcal{O}(10^{-51}) \left(\frac{r_T}{0.06} \right)^{1/2} \left(\frac{\mathcal{A}_R}{2.41 \times 10^{-9}} \right)^{1/2}, \quad (4.27)$$

which is much smaller than the lower limit on H_r imposed throughout this analysis. There is therefore no surprise that $h_0^2 \Omega_{gw}(\nu)$ could be as large as 10^{-10} in the nHz range since from 10^{-14} Hz to 10 nHz there are 6 orders of magnitude and $h_0^2 \Omega_{gw}(\nu)$ may increase, in this range, with linear slope from 10^{-16} to 10^{-10} . Reference [80] demands therefore that the plasma is *not* dominated by radiation by the time of big-bang nucleosynthesis and this approach is totally rejected by the viewpoint conveyed in the present analysis⁹.

The considerations developed in the previous paragraph are also essential for a fair comparison of the relic gravitons discussed here with the cosmic string signals (see, in this respect, the review of Ref. [20]). The gravitational waves emitted by oscillating loops at different epochs have been argued to produce a stochastic background [81] with quasi-flat spectral energy density which is typically larger than the inflationary signal. The nature of the signal changes depending on three basic parameters: the string tension in Planck units (i.e. $G\mu$); the typical size of the loops normalized at the formation time; the emission efficiency of the loop. The quoted values of $G\mu$ may range between 10^{-8} and 10^{-23} while the typical size of the loop may vary between 10^{-10} and 10^{-1} . The large interval of variation of the parameters makes it obvious that different signals can be expected. From symmetry breaking in the grand unified context the typical values of $G\mu$ could be as large as $\mathcal{O}(10^{-6})$. These values would cause however measurable temperature and polarization anisotropies of the CMB and have been ruled out; current limits from CMB observations demand $G\mu < \mathcal{O}(10^{-8})$. For the largest values of $G\mu$ potentially compatible with CMB data the $h_0^2 \Omega_{gw}$ from cosmic strings exhibits a hump in the nHz region [82] (see also [83]) and then flattens out. As $G\mu$ diminishes the hump shifts at higher frequencies and the overall signal is suppressed potentially getting to $h_0^2 \Omega_{gw} = \mathcal{O}(10^{-15})$ for $G\mu = \mathcal{O}(10^{-21})$. Since the relic

gravitons discussed here never lead to a large signal in the nHz region, the only possible ambiguity may arise when $G\mu \ll 10^{-9}$. In this case the nearly flat branch of the cosmic string signal might be confused with situations similar to the one described, for instance, in Fig. 5. A detailed comparison is however beyond the scopes of this paper.

The final point we want to mention concerns the possibility of second-order effects and their interplay with the considerations presented here. In the concordance paradigm where the curvature inhomogeneities are Gaussian and adiabatic the stochastic backgrounds of relic gravitons are corrected by second-order effects that involve an effective anisotropic stress [84] which is however gauge-dependent¹⁰. The tensor modes reentering the Hubble radius when the plasma is dominated by a stiff fluid lead to a spectral energy density whose blue slope depends on the total post-inflationary sound speed. This result gets however corrected by a secondary term coming from the curvature inhomogeneities that reenter all along the same stage of expansion. In comparison with the first-order result, the secondary contribution has been shown to be always suppressed inside the sound horizon and its effect on the total spectral energy density of the relic gravitons is therefore negligible for all phenomenological purposes [86]. The same conclusion applies also in the present situation.

5 Concluding remarks and future perspectives

If the wavelengths that left the Hubble radius during inflation reentered in the radiation-dominated stage of expansion the spectral energy density of the inflationary gravitons is today quasi-flat for typical frequencies larger than 100 aHz. Prior to nucleosynthesis the timeline of the expansion rate is however unknown and we considered here a post-inflationary evolution consisting of a sequence of stages expanding at rates that are alternatively faster and slower than radiation. As a consequence, the spectral energy density can even be eight orders of magnitude larger than the conventional inflationary signal for frequencies between the μ Hz and a fraction of the Hz.

Below the Hz various space-borne detectors will probably be operational in the next twenty years and the signals expected in the mHz region are dominated by astrophysical sources (e.g. galactic white dwarves, solar-mass black holes, supermassive black holes coming from galaxy mergers). The only cosmological sources considered in this context are associated with the phase transitions at the TeV scale

⁸ See, in particular, the two plots in Fig. 8 of Ref. [80] where the lowest break of the spectrum is $\mathcal{O}(10^{-14})$ Hz and possibly even smaller.

⁹ It should also be rejected on a more general ground since it is unclear how it is possible to form the light element abundances in such a context. We remark that the slopes derived by the authors in Eqs. (93)–(94) of Ref. [79] coincide exactly with the ones discussed long ago (see e.g. Eq. (3.32) of Ref. [31]).

¹⁰ It has been noted that the different gauge-dependent results can be swiftly compared by a careful use of the normal modes of the system. It turns out that the results obtained in different gauges is comparable for typical wavelengths shorter than the Hubble radius. See, in this respect, the discussion in Refs. [85, 86].

even if it is well established, both perturbatively and non-perturbatively, that the standard electroweak theory leads to a cross-over regime where drastic deviations from homogeneity (and the consequent bursts of gravitational radiation) should not be expected. The inflationary signal is customarily regarded as irrelevant since its spectral energy density could be at most $h_0^2 \Omega_{gw}(\nu_S, \tau_0) = \mathcal{O}(10^{-17})$ for $r_T \leq 0.06$ and for $\nu_S = \mathcal{O}(\text{mHz})$. The relic gravitons of inflationary origin may instead lead to $h_0^2 \Omega_{gw}(\nu_S, \tau_0) = \mathcal{O}(10^{-9})$ provided the expansion history prior to nucleosynthesis is not constantly dominated by radiation. The slopes of the spectral energy density obtained in the case of a putative strongly first-order phase transition are much steeper than the ones associated with a modified expansion history. When confronted with the most relevant phenomenological bounds the class of signals discussed here is predominantly constrained by the limits on the massless species at the nucleosynthesis scale and by the direct observations of ground-based detectors (i.e. LIGO, Virgo and KAGRA). From the profiles of the spectral energy density and from the slopes of the hump in the mHz range it is possible to infer the post-inflationary expansion history for typical curvature scales that are between $10^{-44} M_P$ and $10^{-34} M_P$ (i.e. roughly 10 orders of magnitude larger than the nucleosynthesis scale). The analysis of the spectral energy density in different frequency ranges (e.g. nHz, mHz and MHz) might even allow to reconstruct the expansion history of the Universe at earlier and later times. It is finally interesting that some regions of the parameter space that are relevant for space-borne detectors also lead to a potentially large signal in the audio band and will probably be directly probed or excluded in the near future.

All in all the perspective conveyed in this analysis suggests that the frequency range below the Hz should be carefully investigated in the light of a possible signal coming from inflationary gravitons. While a strongly first order phase transition may be realized beyond the standard electroweak theory, the present discussion only assumes a conventional inflationary stage supplemented by a post-inflationary evolution that deviates from the conventional radiation dominance prior to nucleosynthesis. The observations in the mHz region could then simultaneously test the occurrence of an early inflationary stage and of a post-inflationary expansion history whose details are still unknown and might only be discovered by looking at the spectra of relic gravitons.

Acknowledgements It is a pleasure to thank T. Basaglia, A. Gentile-Beccot, S. Rohr, J. Vigen and the whole CERN Scientific Information Service for their kind help during the preparation of this manuscript.

Data Availability Statement This manuscript has no associated data or the data will not be deposited. [Authors' comment: This paper has no associated data since it is a theoretical study. The experimental data recall in this study have been already published elsewhere and are quoted in the paper.]

Open Access This article is licensed under a Creative Commons Attribution 4.0 International License, which permits use, sharing, adaptation, distribution and reproduction in any medium or format, as long as you give appropriate credit to the original author(s) and the source, provide a link to the Creative Commons licence, and indicate if changes were made. The images or other third party material in this article are included in the article's Creative Commons licence, unless indicated otherwise in a credit line to the material. If material is not included in the article's Creative Commons licence and your intended use is not permitted by statutory regulation or exceeds the permitted use, you will need to obtain permission directly from the copyright holder. To view a copy of this licence, visit <http://creativecommons.org/licenses/by/4.0/>.

Funded by SCOAP³. SCOAP³ supports the goals of the International Year of Basic Sciences for Sustainable Development.

References

1. L.P. Grishchuk, Sov. Phys. JETP **40**, 409 (1975)
2. L.P. Grishchuk, Zh. Eksp. Teor. Fiz. **67**, 825 (1974)
3. L.P. Grishchuk, Ann. N. Y. Acad. Sci. **302**, 439 (1977)
4. L.H. Ford, L. Parker, Phys. Rev. D **16**, 245 (1977)
5. A.A. Starobinsky, JETP Lett. **30**, 682 (1979)
6. A.A. Starobinsky, Pisma. Zh. Eksp. Teor. Fiz. **30**, 719 (1979)
7. V.A. Rubakov, M.V. Sazhin, A.V. Veryaskin, Phys. Lett. B **115**, 189 (1982)
8. L.F. Abbott, M.B. Wise, Nucl. Phys. B **244**, 541 (1984)
9. B. Allen, Phys. Rev. D **37**, 2078 (1988)
10. V. Sahni, Phys. Rev. D **42**, 453 (1990)
11. L.P. Grishchuk, M. Solokhin, Phys. Rev. D **43**, 2566 (1991)
12. M. Gasperini, M. Giovannini, Phys. Lett. B **282**, 36 (1992)
13. Y. Akrami et al. [Planck Collaboration], Astron. Astrophys. **641**, A10 (2020)
14. N. Aghanim et al. [Planck Collaboration], Astron. Astrophys. **641**, A6 (2020)
15. P.A.R. Ade et al. [BICEP and Keck], Phys. Rev. Lett. **127**, 151301 (2021)
16. S. Weinberg, Phys. Rev. D **69**, 023503 (2004)
17. D.A. Dicus, W.W. Repko, Phys. Rev. D **72**, 088302 (2005)
18. R. Abbott et al. [KAGRA, Virgo and LIGO Scientific], Phys. Rev. D **104**, 022004 (2021)
19. B.P. Abbott et al. [LIGO Scientific and Virgo], Phys. Rev. D **100**, 061101 (2019)
20. M. Giovannini, Prog. Part. Nucl. Phys. **112**, 103774 (2020)
21. P. Amaro-Seoane et al. [LISA], [arXiv:1702.00786](https://arxiv.org/abs/1702.00786) [astro-ph.IM]
22. LISA documents webpage. <https://www.cosmos.esa.int/web/lisa/lisa-documents>
23. N. Seto, S. Kawamura, T. Nakamura, Phys. Rev. Lett. **87**, 221103 (2001)
24. S. Kawamura et al., Class. Quantum Gravity **28**, 094011 (2011)
25. H. Kudoh, A. Taruya, T. Hiramatsu, Y. Himemoto, Phys. Rev. D **73**, 064006 (2006)
26. G.M. Harry et al., Class. Quantum Gravity **23**, 4887 (2006)
27. W.-R. Hu, Y.-L. Wu, Nat. Sci. Rev. **4**, 685 (2017)
28. W.-H. Ruan, Z.-K. Guo, R.-G. Cai, Y.-Z. Zhang, [arXiv:1807.09495](https://arxiv.org/abs/1807.09495)
29. T.J. Luo et al. [TianQin], Class. Quantum Gravity **33**, 035010 (2016)
30. X.C. Hu et al., Class. Quantum Gravity **35**, 095008 (2018)
31. M. Giovannini, Phys. Rev. D **58**, 083504 (1998)
32. M. Giovannini, Phys. Rev. D **60**, 123511 (1999)
33. P.J.E. Peebles, A. Vilenkin, Phys. Rev. D **59**, 063505 (1999)
34. V. Sahni, M. Sami, T. Souradeep, Phys. Rev. D **65**, 023518 (2002)
35. J. Haro, W. Yang, S. Pan, JCAP **01**, 023 (2019)
36. M. Gorghetto, E. Hardy, H. Nicolaescu, JCAP **06**, 034 (2021)

37. B. Li, P.R. Shapiro, JCAP **10**, 024 (2021)
38. L.H. Ford, Phys. Rev. D **35**, 2955 (1987)
39. B. Spokoiny, Phys. Lett. B **315**, 40–45 (1993)
40. M. Giovannini, Phys. Lett. B **668**, 44 (2008)
41. M. Giovannini, Class. Quantum Gravity **26**, 045004 (2009)
42. M. Giovannini, Phys. Rev. D **105**, 103524 (2022)
43. B. Goncharov et al., Astrophys. J. Lett. **917**, L19 (2021)
44. S. Chen et al., Mon. Not. R. Astron. Soc. **508**, 4970 (2021)
45. J. Antoniadis et al., [arXiv:2201.03980](https://arxiv.org/abs/2201.03980) [astro-ph.HE]
46. Z. Arzoumanian et al., Astrophys. J. Lett. **905**, L34 (2020)
47. A.D. Sakharov, Sov. Phys. JETP **22**, 241 (1966)
48. A.D. Sakharov, Zh. Eksp. Teor. Fiz. **49**, 345 (1965)
49. P.J.E. Peebles, J.T. Yu, Astrophys. J. **162**, 815 (1970)
50. T. Hasegawa, N. Hiroshima, K. Kohri, R.S.L. Hansen, T. Tram, S. Hannestad, JCAP **12**, 012 (2019)
51. M. Kawasaki, K. Kohri, N. Sugiyama, Phys. Rev. D **62**, 023506 (2000)
52. A.R. Liddle, S.M. Leach, Phys. Rev. D **68**, 103503 (2008)
53. V.F. Schwartzmann, JETP Lett. **9**, 184 (1969)
54. M. Giovannini, H. Kurki-Suonio, E. Sihvola, Phys. Rev. D **66**, 043504 (2002)
55. R.H. Cyburt, B.D. Fields, K.A. Olive, E. Skillman, Astropart. Phys. **23**, 313 (2005)
56. L. Lentati et al., Mon. Not. R. Astron. Soc. **453**, 2576 (2015)
57. G. Desvignes et al., Mon. Not. R. Astron. Soc. **458**, 3341 (2016)
58. Z. Arzoumanian et al., Astrophys. J. **859**, 47 (2018)
59. Z. Arzoumanian et al. [NANOGrav], Astrophys. J. **821**, 13 (2016)
60. D.A. Kirzhnits, A.D. Linde, Phys. Lett. B **42**, 471 (1972)
61. A.D. Linde, Rep. Prog. Phys. **42**, 389 (1979)
62. K. Kajantie, M. Laine, K. Rummukainen, M.E. Shaposhnikov, Phys. Rev. Lett. **77**, 2887 (1996)
63. F. Csikor, Z. Fodor, J. Heitger, Phys. Rev. Lett. **82**, 21 (1999)
64. A. Kosowsky, M.S. Turner, Phys. Rev. D **47**, 4372 (1993)
65. S.J. Huber, T. Konstandin, JCAP **09**, 022 (2008)
66. T. Konstandin, JCAP **03**, 047 (2018)
67. D. Cutting, M. Hindmarsh, D.J. Weir, Phys. Rev. D **97**, 123513 (2018)
68. M. Giovannini, Class. Quantum Gravity **34**, 135010 (2017)
69. M. Giovannini, Phys. Rev. D **61**, 063004 (2000)
70. M. Giovannini, Phys. Rev. D **61**, 063502 (2000)
71. V. Braginsky, M. Menskii, Pis'ma. Zh. Eksp. Teor. Fiz. **13**, 585 (1971)
72. V. Braginsky, M. Menskii, JETP Lett. **13**, 417 (1971)
73. F. Pegoraro, L. Radicati, Ph. Bernard, E. Picasso, Phys. Lett. A **68**, 165 (1978)
74. A.M. Cruise, Class. Quantum Gravity **17**, 2525 (2000)
75. F.Y. Li, M.X. Tang, D.P. Shi, Phys. Rev. D **67**, 104008 (2003)
76. R. Ballantini, P. Bernard, A. Chincarini, G. Gemme, R. Parodi, E. Picasso, Class. Quantum Gravity **21**, S1241 (2004)
77. A.M. Cruise, R.M. Ingle, Class. Quantum Gravity **23**, 6185 (2006)
78. A. Nishizawa et al., Phys. Rev. D **77**, 022002 (2008)
79. S.S. Mishra, V. Sahni, A.A. Starobinsky, JCAP **05**, 075 (2021)
80. M.R. Haque, D. Maity, T. Paul, L. Sriramkumar, Phys. Rev. D **104**, 063513 (2021)
81. A. Vilenkin, Phys. Lett. B **107**, 47 (1981)
82. J.J. Blanco-Pillado, K.D. Olum, X. Siemens, Phys. Lett. B **778**, 392 (2018)
83. J.J. Blanco-Pillado, K.D. Olum, B. Shlaer, Phys. Rev. D **83**, 083514 (2011)
84. K.N. Ananda, C. Clarkson, D. Wands, Phys. Rev. D **75**, 123518 (2007)
85. M. Giovannini, Int. J. Mod. Phys. A **35**(27), 2050165 (2020)
86. M. Giovannini, Phys. Lett. B **810**, 135801 (2020)